



**HAL**  
open science

## Analyse fréquentielle des débits de crues avec des données historiques en prenant en compte les erreurs aléatoires et systématiques

Luc Neppel, Benjamin Renard, Michel Lang, Pierre Alain Ayrat, Denis Coeur, Eric Gaume, Nicolas Jacob, Olivier Payrastre, Karine Pobanz, Freddy Vinet

### ► To cite this version:

Luc Neppel, Benjamin Renard, Michel Lang, Pierre Alain Ayrat, Denis Coeur, et al.. Analyse fréquentielle des débits de crues avec des données historiques en prenant en compte les erreurs aléatoires et systématiques. *Hydrological Sciences Journal*, 2010, 55 (2), pp 192-208. 10.1080/02626660903546092 . hal-00509088

**HAL Id: hal-00509088**

**<https://hal.science/hal-00509088v1>**

Submitted on 15 May 2020

**HAL** is a multi-disciplinary open access archive for the deposit and dissemination of scientific research documents, whether they are published or not. The documents may come from teaching and research institutions in France or abroad, or from public or private research centers.

L'archive ouverte pluridisciplinaire **HAL**, est destinée au dépôt et à la diffusion de documents scientifiques de niveau recherche, publiés ou non, émanant des établissements d'enseignement et de recherche français ou étrangers, des laboratoires publics ou privés.

1 **Flood frequency analysis using historical data: accounting for random and systematic**  
2 **errors**

3

4 LUC NEPPEL<sup>1</sup>, BENJAMIN RENARD<sup>2</sup>, MICHEL LANG<sup>2</sup>, PIERRE-ALAIN AYRAL<sup>3</sup>,  
5 DENIS COEUR<sup>4</sup>, ERIC GAUME<sup>5</sup>, NICOLAS JACOB<sup>6</sup>, OLIVIER PAYRASTRE<sup>7</sup>, KARINE  
6 POBANZ<sup>2</sup>, FREDDY VINET<sup>8</sup>.

7 1 UMR HydroSciences Montpellier – Université Montpellier II – place Eugène Bataillon – CC MSE – 34090  
8 Montpellier Cedex 5, France. – [neppel@msem.univ-montp2.fr](mailto:neppel@msem.univ-montp2.fr)

9 2 Cemagref Lyon – Hydrology Hydraulics – 3 bis quai Chauveau – CP 220 – 69336 Lyon cedex 09, France.

10 3 Ecole des Mines d'Alès, LGEI, 6 av de Clavières, 30 100 Alès, France

11 4 ACTHYS Diffusion, 253, chemin de Plate-Rousset, 38 330 Biviers, France

12 5 LCPC, Route de Bouaye, BP 4129, 44341 Bouguenais cedex, France

13 6 Université de Lyon II - UMR 5600 – 5 avenue Pierre Mendès –France 69676 Bron cedex, France

14 7 SPC Grand Delta du Rhone, DDE du Gard, 89, rue Weber, 30907 Nimes cedex, France

15 8 UMR Gester,, Université Montpellier III, Route de Mende, 34199 Montpellier Cedex 5, France

16 **Abstract :**

17

18 This paper presents a flood frequency analysis (FFA) based on a set of systematic data and a  
19 set of historical floods, applied to several Mediterranean catchments. After identification and  
20 collection of data on historical floods, several hydraulic models were constructed to account  
21 for geomorphological changes. Recent and historical rating curves were constructed and  
22 applied to reconstruct flood discharge series along with their uncertainty. This uncertainty  
23 stems from two types of errors: (a) random errors related to the water level readings; (b)  
24 systematic errors related to over- or underestimation of the rating curve. A Bayesian  
25 frequency analysis is performed to take both sources of uncertainty into account. It is shown  
26 that: (a) the uncertainty affecting discharges should be carefully evaluated and taken into  
27 account in the FFA, as it can increase the quantiles confidence interval; (b) the quantiles are

28 found consistent with the ones obtained with empirical methods, for two out of four of the  
29 catchments.

30

31 **Keyword :**

32

33 Historical flood, Bayesian flood frequency analysis, discharge errors, Mediterranean  
34 catchment

35

## 36 **I. INTRODUCTION**

37

38 The most widely used method for flood frequency analysis is to estimate the parameters of a  
39 probability distribution using a sample of observed flood events. As discharge time series are  
40 often short compared to the recurrence interval of the quantiles of interest, this method is  
41 highly sensitive to the sampled data. In France, for example, the longer uninterrupted  
42 discharge series provide 40 to 50 years of data, with only a couple of series longer than 80  
43 years (Renard, 2006), whereas flood-risk areas are defined on the basis of a design event with  
44 a recurrence interval of at least 100 years. One way of reducing the resulting uncertainties is  
45 to extend the observation period by augmenting the systematic observations with historical  
46 flood events or paleofloods. A number of applications – for example, Llasat *et al.* (2005) in  
47 Catalonia; Naulet *et al.* (2005) on the Ardèche river (France); and Payrastre *et al.* (2005,  
48 2006) on small watersheds in the Aude river system (France) – demonstrate the improvement  
49 offered by this method compared to methods using only the systematic observation period.  
50 Brazdil *et al.* (2006) provide a more detailed assessment of flood risk that takes account of  
51 historical flood events in Europe.

52 A first difficulty with this approach lies in the estimation of empirical flood frequencies from  
53 a sample made of both systematic and censored data. Indeed, historical discharge data are not  
54 exhaustive: only events exceeding a given threshold of perception (possibly varying over  
55 time) are reported. Hirsh and Stedinger (1987) and Naulet (2002) propose ways of computing  
56 empirical flood frequencies with a mixed systematic/censored sample. A second difficulty is  
57 to quantify the discharge of historical flood events, as this information is often subject to  
58 considerable uncertainty, which must be taken into consideration in estimating flood  
59 frequency. Moreover, such error is not limited to historical floods; it also affects more recent  
60 exceptional events for which only posterior estimates of discharge are available (Gaume *et al.*,  
61 2004; Sheffer *et al.*, 2008). It can be considered that the data on historical flood events are  
62 marred by random errors related to readings of the staff gauge, and both historical and recent  
63 flood events are marred by systematic errors arising from over- or underestimation of the  
64 rating curve.

65 This paper presents a frequency analysis method that takes these two sources of error into  
66 account for floods in both the historical and systematic periods. The approach presented was  
67 developed under the INONDHIS-LR project (Neppel *et al.*, 2007), funded by the French  
68 Ministry of Ecology. The second section presents the study area and the data. The third  
69 section describes the frequency analysis models, with an application to a Mediterranean  
70 catchment. The results of the analysis are further discussed in the fourth section.

71

## 72 **II. STUDY AREA AND DATA**

73

### 74 **1. Location of the study area**

75

76 The INONDHIS-LR project studies ten Mediterranean catchments: two in the Hérault river  
77 system, four in the Aude and four in the Gard watershed. This paper considers the latter  
78 catchments, particularly the catchment of the Gardon d'Anduze river at Anduze, which has an  
79 area of 540 km<sup>2</sup>, making it – along with the Gardon d'Alès (320 km<sup>2</sup>) – one of the main  
80 tributaries of the Gard river, which drains a total area of about 2000 km<sup>2</sup> into the Rhône river  
81 (Figure 1).

82

83 The two main tributaries of the Gardon d'Anduze are the Gardon de Saint-Jean (154 km<sup>2</sup>) and  
84 the Gardon de Mialet (219 km<sup>2</sup>). Their catchments are bounded on the north by the crests of  
85 the Cévennes range, which can exceed 1000 mNGF<sup>1</sup> in altitude, and their outlets lie at  
86 altitudes around 100 m. Given the steep gradients of the catchments and the torrential rainfall  
87 characteristic of the Mediterranean rim in autumn, these streams are the site of devastating  
88 floods (Ayrat, 2004; Marchandise, 2007).

89

90 The four catchments in the Gard system are instrumented by gauging stations belonging to the  
91 Grand Delta flood forecasting department (FFD), formerly the flood warning department  
92 (FWD), founded in 1892. The purpose of these measurements was not to compile a time  
93 series of discharge data for hydrological analysis, but to provide flood warning. Managers  
94 were therefore interested in the flood crest levels rather than in discharge *per se*, which  
95 explains the virtual absence of gaugings (there are only two low-flow gaugings at the Anduze  
96 station). The possibilities for gauging discharge during flood events are severely limited by  
97 the high flow velocity. Incidentally, this is why a majority of hydrometric stations in the  
98 Mediterranean region are not gauged beyond the 2-year flood (Lang *et al.*, 2006). The Grand  
99 Delta FFD allowed the authors of this paper to use the topographical surveys conducted in

---

<sup>1</sup> NGF = *nivellement général de la France*, the altitude reference system of France's National Geographical Institute (IGN).

100 2003 for all catchments in the Gard river system, with longitudinal profiles and latitudinal  
101 profiles from 40 to 300 metres apart.

102

## 103 **2. Available historical data**

104

105 The work of identifying historical information, collecting it from archives and subjecting it to  
106 critical analysis was conducted in conjunction with historians and geographers. The methods  
107 used are not described in this paper; for a description, see Cœur *et al.* (2002) or Naulet *et al.*  
108 (2005). The data relate either to flood crest levels or to the morphology of the Gardon.

109

110 For this sector, a total of 249 useable flood crest measurements were found, the oldest dating  
111 from 1741. When their positions were given with respect to a landmark still in existence, it  
112 became possible to place them in the NGF system. Some archives provided only censored  
113 information owing to the lack of precision of observations, e.g. “the water level is above the  
114 bridge parapet”. Figure 2 lists all the flood events found for the Gardon d’Anduze; the series  
115 is incomplete for the 1741-1891 period (high water mark, threshold level not exceeded,  
116 measurement recorded as an interval) and complete since 1892. The FFD archives contributed  
117 greatly: the entire series of daily water-level measurements were found for the four  
118 catchments studied, dating back to the founding of FWD in 1892. The past positions and zero  
119 levels of the staff gauges were reconstructed, partly from correspondence between FFD  
120 engineers and the observers assigned to each sector, and partly from breaks in the time series  
121 of low-water levels.

122

123 Historical information on the morphology of the Gardon stems from technical studies for  
124 hydraulic works and reports on major hydrometeorological events. The plans, consisting of

125 longitudinal profiles and a few latitudinal profiles, show the crest levels of known major flood  
126 events. The period from 1845-1850 to the present, was marked by a deepening of the  
127 streambeds, by more than three metres in some areas. This phenomenon, which has also been  
128 evidenced in a nearby area through analysis of lichens (Gob *et al.*, 2008), results from an  
129 incision in the gravelly alluvium and the gradual scouring out of this material once  
130 sedimentary build-up in the channels stopped in these catchments. As in most watercourses in  
131 the Rhône watershed, the process seems irreversible as from the 1950s. Figure 3 presents a 3  
132 km stretch of the Gardon d'Anduze at Anduze. Comparing the oldest useable profile, dating  
133 from 1849, to that produced in the 2003 survey, it can be seen that the river bed has sunk by  
134 approximately 2 m on the downstream side of the Anduze bridge.

135

### 136 **3. Example of reconstruction of flood discharges at Anduze**

137

138 Estimates of flood discharge are based on hydraulic modelling of a reach about 2 km long.  
139 The river bed was fairly stable at the downstream end between the 1849 and 1985 profiles  
140 (Figure 3), then deepened by about 1.5 m between 1985 and 2003. We therefore use two  
141 models: a “recent” model based on the 2003 topographical surveys supplemented by  
142 Cemagref's 2006 surveys and applied to the period from 1985 onward; and a “historical”  
143 model obtained by raising the river bed floor by 1.50 m. Considering the consistency between  
144 1849 and 1985 profiles, the latter is considered to be representative of the streambed  
145 topography for the historical period. The historical profiles collected did not allow to  
146 reconstruct the river's topographical past with sufficient precision to refine the hydraulic  
147 models further.

148

149 Discharge estimates are based on numerical solutions of Barré de Saint Venant's free surface  
150 runoff equations (Chow, 1960), in a one-dimensional simulation using the Manning-Strickler  
151 discharge formula. The software used was RUBARBE (Paquier and Khodashenas, 2002),  
152 which divides the river's geometry into a low flow channel and a floodplain. The software  
153 makes it possible to model a change from sub-critical flow to torrential flow.

154

155 The first step in hydraulic modelling is to calibrate the model, i.e. to determine the Manning  
156 coefficients. The calibration procedure is performed in two steps (main channel/floodplain),  
157 and is described in greater detail in Renouf *et al.* (2005) and Lang *et al.* (2006). For the main  
158 channel, calibration is performed using stream gaugings. A first Manning coefficient is  
159 estimated based on the (water level;discharge) observations. An uncertainty of +/-5 cm for  
160 water level and +/-10% for discharge is then considered. A second calibration procedure is  
161 performed using the values (water level minus 5 cm, discharge plus 10%) and (water level  
162 plus 5 cm, discharge minus 10%). This leads to an interval for the Manning coefficient in the  
163 main channel, which corresponds to an envelop curve of the rating curve (Figure 4). This  
164 approach is applied with two gaugings available at Anduze, corresponding to low discharges  
165 in the main channel. The corresponding Manning coefficient ranges from 1/30 to 1/20. In the  
166 floodplain, no measurements were available, so the Manning coefficient is restricted to the  
167 interval 1/20- 1/10, based on field observations and the configuration of the floodplain (see  
168 correspondence tables, Barnes, 1967).

169

170 The second step is to construct rating curves in the staff gauge cross-section. For each model  
171 (historical and recent), the primary relationship between discharge and water level is  
172 determined, then a range for this relationship is derived from the uncertainty bounds on the  
173 Manning coefficient, as explained on figure 4. Figure 5 presents the rating curves obtained.



174 One can notice on figure 5 that the upper limit of the rating curve described by the rating  
175 curve error model doesn't correspond to the previous one by hydraulic sensitivity analysis (i.e  
176 the envelop curve related to the sensitive analysis on Manning coefficient). The hydraulic  
177 analysis showed that if supercritical flow appears in the neighbourhood of the bridge for the  
178 three curves (respect. upper, central and lower) for respectively  $Q = 4000$ ,  $5000$  and  $6000$   
179  $m^3/s$ , the position of the hydraulic jump is either just in front of the flood scale (upper curve)  
180 or upstream the flood scale (central and lower curves). The former case leads to an equivocal  
181 relationship between stage and discharge, but a large uncertainty remains on the exact  
182 location of the hydraulic jump. As such hypothetical upper limit yields values that are much too  
183 high in terms of specific discharge, it has been considered to be overestimated. The rating  
184 curve error model was therefore calibrated without hydraulic jump.

185  
186 Once the rating curves have been constructed for both the recent and historical models, the  
187 sample of flood level measurements is used to construct the sample of discharge values.  
188 Figure 2 shows the series of reconstructed discharge values from 1741 to 2005. Discharges  
189 have been estimated using the central rating curves in figure 5 (the uncertainty related to a  
190 possible systematic rating curve error is therefore not represented in figure 2). It can be  
191 observed that this data series is made of several data types:

- 192 • Point-values (circles) correspond to water level data known with high precision.  
193 Discharges corresponding to such data are therefore solely affected by the uncertainty  
194 stemming from rating curve errors (not represented in figure 2).
- 195 • Intervals correspond to water level data known with limited precision. The  
196 information therefore consists of lower and upper bounds for the water level reached  
197 during the flood. This water level interval can be transformed into a discharge interval  
198 using the central rating curve.

199 • The perception threshold (horizontal line) corresponds to the water level ensuring the  
200 exhaustiveness of historical data collection. In other words, it can be ensured that  
201 water levels did not exceed the perception threshold during years with no available  
202 information in figure 2 (otherwise, such event would have been recorded in the  
203 historical archives).

204

205 The five highest flood levels recorded at Anduze are those of 1958 (7.6 m; 4575 m<sup>3</sup>/s), 1861  
206 which ranked between 7m (4100 m<sup>3</sup>/s) and 8.2 m (5600 m<sup>3</sup>/s), 1890 (7.1 m; 4260 m<sup>3</sup>/s), 1846  
207 and 1847 (7.0 m; 4135 m<sup>3</sup>/s). For the flood event of 9 September 2002, the gauge reading was  
208 initially recorded as 7.60 m in the FWD survey, but a review led to it being adjusted to and  
209 ultimately validated at 5.60 m with hydraulic modelling, as the initial reading proved  
210 inconsistent with the high-water marks available in the vicinity. The interpretation adopted  
211 jointly with the FFD is that the reading was taken upstream of the Anduze road bridge,  
212 whereas the gauge is downstream. Given the very rough profile of the channel, the hydraulic  
213 model yields an estimate of 3500 m<sup>3</sup>/s with a very large error interval [2590 ; 5870 m<sup>3</sup>/s]. It  
214 should be noted that the value of 6180 m<sup>3</sup>/s that would have been obtained at Anduze (540  
215 km<sup>2</sup>) at a flood crest of 7.60 m would also have been inconsistent from a hydrological  
216 standpoint when compared with the discharge estimate made by the FFD further downstream  
217 at Russans (1515 km<sup>2</sup>), which gave a range of 6000-6800 m<sup>3</sup>/s. The discharge interval used,  
218 [2590, 5870 m<sup>3</sup>/s], agrees with other estimates performed by DDE (2003) and the engineering  
219 firm ISL (2005), which range from 3000 and 3400 m<sup>3</sup>/s.

220

221 The flood of 9 September 2002 merits more detailed analysis because this event caused 23  
222 deaths and an estimated €1.2 billion in damage (Huet *et al.*, 2003). In the upstream part of the  
223 Gardon d'Anduze catchment, this flood is not listed as a major event, while that of 1958

224 remains the biggest since 1741. This is consistent with the rainfall pattern that caused the  
225 2002 flood, which was characterised by very high accumulations on the intermediate part of  
226 the catchment (Delrieu *et al.*, 2004), in contrast to the event of 1958, when the greatest  
227 cumulative rainfall was located in the foothills of the Cévennes range, upstream from Anduze  
228 (Jacquet, 1959). On the downstream part of the catchment, the flood is noteworthy for its  
229 geographical scope and an epicentre of over 600 mm at Lédignan (Neppel *et al.*, 2003).  
230 However, a paleohydrological analysis by Sheffer *et al.* (2008) in the canyons of the Gardon  
231 shows that the 2002 flood level has been exceeded at least five times over the last 500 years,  
232 based on sediment traces and dating of organic and mineral particles.

233

234

### 235 **III. FREQUENCY ANALYSIS OF FLOOD DATA**

236

237 The aim is to estimate flood quantiles from the samples collected for the recent and historical  
238 periods. This estimate needs to take account of the fact that the data are incomplete and that  
239 the discharge values are estimated using a hydraulic model and subject to considerable  
240 uncertainty.

241 The estimation of flood quantiles can be based on data extracted from two distinct sampling  
242 approaches. The peak-over-threshold (POT) approach uses flood peaks exceeding a  
243 predefined threshold. Since the exhaustiveness of data from the historical period is related to a  
244 perception threshold, it seems natural to use a POT approach, with a first exceedance  
245 threshold equal to the perception threshold during the historical period, and a second, lower,  
246 exceedance threshold during the systematic period. An example of POT-analysis of historical  
247 data can be found in the paper by Parent and Bernier (2003). Alternatively, historical data can  
248 also be included in the analysis of annual maxima (AM, see e.g. Naulet *et al.*, 2006). The

249 perception threshold is considered as a censoring threshold in this case. In this study, we  
250 opted for the AM approach.

251 The pros and cons of each approach for analyzing historical data are still unclear. An obvious  
252 drawback of the AM approach would be the loss of data if two (or more) floods happened to  
253 exceed the perception threshold within the same year. However, this is unlikely to occur with  
254 high perception thresholds. In particular, this did not occur in the dataset studied in this paper.  
255 A formal evaluation of the relative merits of the AM and POT approaches for analysing  
256 historical data would be of great interest; however, it is considered to lie beyond the scope of  
257 the present paper and is left for future work.

258 Let  $X_t$  be the random variable representing the “true” annual maximum discharge at the  
259 gauging station for year  $t$  ( $t = 1, \dots, T$ ). Extreme value theory suggests using a generalized  
260 extreme value (GEV) distribution to model such data (e.g., Embrecht *et al.*, 1997). The  
261 probability density function  $f$  (pdf) and the cumulative density function  $F$  (cdf) of a  
262  $GEV(\mu, \lambda, \xi)$ , where  $\mu$ ,  $\lambda$  and  $\xi$  are respectively the location, scale and shape parameters, are  
263 given by:

264

$$f(x | \mu, \lambda, \xi) = (1/\lambda) [1 - \xi(x - \mu)/\lambda]^{1/\xi - 1} \exp\left\{-[1 - \xi(x - \mu)/\lambda]^{1/\xi}\right\} \quad (1)$$

$$F(x | \mu, \lambda, \xi) = \exp\left\{-[1 - \xi(x - \mu)/\lambda]^{1/\xi}\right\}$$

$$\lambda > 0; \xi \neq 0; 1 - \xi(x - \mu)/\lambda > 0$$

265

266 The case  $\xi = 0$  corresponds to the Gumbel distribution, and is equal to the limit of equation

267 (1) when  $\xi \rightarrow 0$ :

268

$$f(x|\mu, \lambda) = (1/\lambda) \exp\left\{-\frac{(x-\mu)}{\lambda} - \exp\left(-\frac{(x-\mu)}{\lambda}\right)\right\} \quad (2)$$

$$F(x|\mu, \lambda) = \exp\left\{-\exp\left(-\frac{(x-\mu)}{\lambda}\right)\right\}$$

$$\lambda > 0$$

269

270 The main task of frequency analysis is to estimate the parameter vector  $\theta = (\mu, \lambda, \xi)$ . A  
 271 Bayesian approach is used in this paper (e.g., Gelman et al., 1995). Standard frequency  
 272 analyses usually neglect the possible errors corrupting observed data. In this case, the  
 273 posterior distribution  $p(\theta|X)$  is simply obtained by combining prior information on the  
 274 distribution of the parameters  $p(\theta)$  and the likelihood of the observations vector  $X=(X_t)_{t=1,\dots,n}$ ,  
 275 written as  $p(X|\theta)$ :

276

$$p(\theta|X) = \frac{p(X|\theta)p(\theta)}{\int p(X|\theta)p(\theta)d\theta} \propto p(X|\theta)p(\theta) \quad (3)$$

277 where the symbol ‘ $\propto$ ’ denotes proportionality.

278

### 279 1. Error model

280 Unfortunately, the assumption that observed runoff data are error-free is untenable in most  
 281 applications involving historical data. An error model linking the “true” runoff  $X_t$  (which is  
 282 unknown, but whose distribution is wanted) with the “observed” runoff  $\tilde{X}_t$  (derived from a  
 283 hydraulic model) is needed. Further notation needs to be defined for this purpose.

284 Let  $H_t$  be the “true” water level reached during the highest flood of year  $t$ , and  $\tilde{H}_t$  the  
 285 corresponding observed level. When the historical information collected is deemed accurate  
 286 enough, or for data in the systematic measurement period, the error affecting observed water  
 287 level may be neglected, leading to the assumption  $H_t = \tilde{H}_t$ . However, incomplete information

288 may lead to relax this assumption, by simply assuming the true level is contained in an  
289 interval. This can be formalized as follows:

$$H_t = \tilde{H}_t + \delta_t, \delta_t \in [-l_t; l_t] \quad (4)$$

290 Using the above convention, the observed level  $\tilde{H}_t$  is the centre of the interval of length  $2l_t$ .

291 Importantly, it will be assumed that the errors  $\delta_t$  are independent from year to year. The  
292 rationale behind this assumption is that such errors are due to incompleteness or inconsistency  
293 of the historical information. The error made at year  $t$  should therefore not impact the error at  
294 year  $t+1$ , since it only depends on the availability and consistency of historical information.

295 Runoff data are then derived by applying the rating curve obtained from the hydraulic model  
296 to the observed levels. Since several rating curves may be used, let  $\hat{\psi}_k(h)$  denote the  $k$ th  
297 rating curve ( $k = 1, \dots, N_c$ ).  $\hat{\psi}_k(h)$  is an approximation of the “true” rating curve  $\psi(h)$  linking  
298 the true runoff with the true water level. The following error model will be used to describe  
299 the error made during this approximation:

$$\psi(h) = \gamma_k \hat{\psi}_k(h) \quad (5)$$

300 This multiplicative error model is justified by the common observation that absolute rating  
301 curve errors (differences between true and estimated discharges) increase with the discharge  
302 value (e.g., Thyer et al., 2009; Reitan and Petersen-Overleir, 2009). Contrarily to water level  
303 errors, the rating curve error is systematic, i.e. all runoff data included in the period of validity  
304 of the  $k$ th rating curve are affected by the same multiplicative error  $\gamma_k$ . This error model is a  
305 particular case of the rating curve error model proposed by Kuczera (1996).

306 Combining equations (4) and (5) allows deriving the relationship between true and observed  
307 runoff as follows:

$$\begin{aligned}
 X_t &= \psi(H_t) & (6) \\
 &= \gamma_k \hat{\psi}_k(H_t) \\
 &= \gamma_k \hat{\psi}_k(\tilde{H}_t + \delta_t) \\
 &= \gamma_k \left[ \hat{\psi}_k(\tilde{H}_t) + \hat{\psi}_k(\tilde{H}_t + \delta_t) - \hat{\psi}_k(\tilde{H}_t) \right] \\
 &= \gamma_k \left[ \tilde{X}_t^{(k)} + \hat{\psi}_k(\tilde{H}_t + \delta_t) - \hat{\psi}_k(\tilde{H}_t) \right] \\
 &= \gamma_k \left[ \tilde{X}_t^{(k)} + \varepsilon_t \right], \\
 &\text{with } \varepsilon_t = \hat{\psi}_k(\tilde{H}_t + \delta_t) - \hat{\psi}_k(\tilde{H}_t)
 \end{aligned}$$

308 The superscript ( $k$ ) has been introduced to recall the rating curve used to derive the observed  
 309 runoff  $\tilde{X}_t^{(k)}$ . Since the additive water level error  $\delta_t$  is included in the interval  $[-l_t; l_t]$ , the  
 310 resulting additive runoff error  $\varepsilon_t$  is included in the interval  
 311  $[\hat{\psi}_k(\tilde{H}_t - l_t) - \hat{\psi}_k(\tilde{H}_t); \hat{\psi}_k(\tilde{H}_t + l_t) - \hat{\psi}_k(\tilde{H}_t)] = [a_t; b_t]$ .

312 The error model in equation (6) shows that observed runoff is affected by two different types  
 313 of errors: a multiplicative systematic error stemming from the estimated rating curve, and  
 314 independent event-specific errors stemming from the imperfect knowledge of the water level  
 315 reached during historical floods.

316

## 317 2. Parameter estimation

318 In order to perform the Bayesian estimation of the GEV parameters, the likelihood of the  
 319 observations  $\tilde{X}_t^{(k)}$  needs to be derived. In a first step, inverting equation (6) gives the  
 320 following relationship:

321

$$\tilde{X}_t^{(k)} = X_t / \gamma_k - \varepsilon_t \quad (7)$$

322 It is then possible to demonstrate that  $p(\tilde{X}_t^{(k)} | \mu, \lambda, \xi, \gamma_k, \varepsilon_t)$ , the distribution of an  
 323 observation  $\tilde{X}_t^{(k)}$ , conditionally on errors  $\gamma_k$  and  $\varepsilon_t$ , is a  $GEV(\mu / \gamma_k - \varepsilon_t, \lambda / \gamma_k, \xi)$  (see  
 324 appendix 1).

325 The explicit treatment of errors leads to the introduction of additional unknown terms in the  
 326 inference, namely vectors  $\boldsymbol{\gamma}=(\gamma_1,\dots,\gamma_{Nc})$  and  $\boldsymbol{\varepsilon}=(\varepsilon_1,\dots,\varepsilon_T)$ . The length of vector  $\boldsymbol{\gamma}$  is equal to the  
 327 number of rating curves  $Nc$  used to reconstruct past discharges, which is likely to remain  
 328 relatively small. However, the length of vector  $\boldsymbol{\varepsilon}$  can theoretically be equal to the total number  
 329 of years included in the analysis  $T$ . In practice, some components of  $\boldsymbol{\varepsilon}$  can be fixed to zero,  
 330 corresponding to flood events whose water levels are assumed to be known without any error  
 331 (circles in Figure 2).

332 There are two options for treating these additional unknown terms: they can be included in the  
 333 list of parameters to be estimated, or alternatively, they can be integrated out from the  
 334 conditional distribution  $p(\tilde{X}_t^{(k)} | \mu, \lambda, \xi, \gamma_k, \varepsilon_t)$  prior to the inference (e.g., *Kuczera, 1992*). In  
 335 this paper, a mixed approach is adopted: parameter vector  $\boldsymbol{\gamma}$  is included in the inference, but  $\boldsymbol{\varepsilon}$   
 336 is integrated out as follows:

$$p(\tilde{X}_t^{(k)} | \mu, \lambda, \xi, \gamma_k) = \int p(\tilde{X}_t^{(k)} | \mu, \lambda, \xi, \gamma_k, \varepsilon_t) p(\varepsilon_t) d\varepsilon_t \quad (8)$$

337 Applying equation (8) requires defining a prior probability distribution for the error term  $\varepsilon_t$ .  
 338 Since  $\varepsilon_t$  is assumed to be included in the interval  $[a_t; b_t]$ , a natural choice is to use the uniform  
 339 distribution on this interval. This choice is particularly interesting because it allows  
 340 performing the integration in equation (8) analytically (see appendix 2). Under this  
 341 assumption, the distribution of an observation  $\tilde{X}_t^{(k)}$ , conditionally on errors  $\gamma_k$  only, is given  
 342 by:

$$p(\tilde{X}_t^{(k)} | \mu, \lambda, \xi, \gamma_k) = \frac{1}{b_t - a_t} \left[ F(\tilde{x}_t^{(k)} + b_t | \mu / \gamma_k, \lambda / \gamma_k, \xi) - F(\tilde{x}_t^{(k)} + a_t | \mu / \gamma_k, \lambda / \gamma_k, \xi) \right] \quad (9)$$

343 Note that in the particular case where  $\varepsilon_t$  is forced to zero (no water-level-related error), the  
 344 conditional distribution  $p(\tilde{X}_t^{(k)} | \mu, \lambda, \xi, \gamma_k)$  is simply given by:



$$p(\tilde{X}_t^{(k)} | \mu, \lambda, \xi, \gamma_k) = f(\tilde{x}_t^{(k)} | \mu / \gamma_k, \lambda / \gamma_k, \xi) \quad (10)$$

345 which appears to be the limit of the right hand side of equation (9) when  $a_t \rightarrow b_t$ .  
 346 Equations (9) and (10) can then be used to derive the likelihood function of the whole set of  
 347 observations  $\mathbf{X}$ . For a given rating curve ( $k$ ), let  $S_k$  be the set of years included in the period of  
 348 validity of the rating curve for which an observation is available (either with point or interval  
 349 water level data, corresponding to circles and intervals in figure 2). Let us further assume that  
 350  $n_k$  years correspond to censored data, i.e. the only available information is that the annual  
 351 maximum flood did not exceed the perception threshold  $u_k$ . Lastly, it is assumed that annual  
 352 maxima are independent and identically distributed. Under these assumptions, following Reis  
 353 and Stedinger (2005), the likelihood function is proportional to:

$$p(\mathbf{X} | \mu, \lambda, \xi, \gamma) \propto \prod_{k=1, Nc} \left[ \prod_{t \in S_k} \{ p(\tilde{X}_t^{(k)} | \mu, \lambda, \xi, \gamma_k) \} \right] [F(u_k | \mu / \gamma_k, \lambda / \gamma_k, \xi)]^{n_k} \quad (11)$$

354 In equation (11), the term  $F(u_k | \mu / \gamma_k, \lambda / \gamma_k, \xi)$  is the cdf of the GEV distribution evaluated  
 355 at the perception threshold, and corresponds to the contribution of a censored data (i.e. below  
 356 the threshold) to the likelihood. The term  $p(\tilde{X}_t^{(k)} | \mu, \lambda, \xi, \gamma_k)$  corresponds to the contribution  
 357 of an observation to the likelihood. It is evaluated with equation (9) or (10) for interval or  
 358 point data, respectively.

359 Assuming prior independence, the posterior pdf can then be derived (up to a constant of  
 360 proportionality) as follows:

$$\begin{aligned} p(\mu, \lambda, \xi, \gamma | \mathbf{X}) &\propto p(\mathbf{X} | \mu, \lambda, \xi, \gamma) p(\mu, \lambda, \xi, \gamma) \\ &\propto p(\mathbf{X} | \mu, \lambda, \xi, \gamma) p(\mu) p(\lambda) p(\xi) \prod_{k=1, Nc} p(\gamma_k) \end{aligned} \quad (12)$$

361 In this case study, the joint prior distribution of the three GEV parameters is obtained by  
 362 assuming their prior independence and by using very broad, uniform distributions for location  
 363 ( $\mu$ ) and scale ( $\lambda$ ) parameters. For the shape parameter  $\xi$ , we use a Gaussian distribution  
 364 centred on zero with a standard deviation of 0.3, which means that the interval  $[-0.6 ; 0.6]$

365 contains over 90% of the prior density. Such a prior distribution for the shape parameter is  
366 similar to the “geophysical prior” of Martins and Stedinger (2000). Thus:

$$p(\mu, \lambda, \xi) = U(\mu | -10000, 10000) U(\lambda | 0, 10000) N(\xi | 0, 0.3^2) \quad (13)$$

367 The assumption of prior independence is mainly used here for convenience. However, since  
368 flat priors are used for the location and scale parameters in order to reflect the lack of prior  
369 knowledge on these parameters, it seems natural not to introduce any form of dependence  
370 between them. Importantly, prior independence does not imply that the parameter posterior  
371 distributions will be independent (i.e., the parameter estimates might be dependent).  
372 Moreover, methods for specifying an informative prior distribution (without necessarily using  
373 the assumption of prior independence) have been proposed (e.g. Coles and Powell, 1996;  
374 Renard et al., 2006a; Ribatet et al., 2006) and could be used within this inference framework.

375  
376 The prior distributions of rating curve error parameters  $\gamma$  remains to be specified. This can be  
377 done using the results of the hydraulic sensitivity study (Figure 5). More accurately, a  
378 triangular prior distribution is used (Figure 6). The mode of this distribution is obtained for  
379  $\gamma=1$  (no error), while the base expands between values *min* and *max*. These values are  
380 determined so that the corresponding rating curves (thick lines in figure 4) roughly match the  
381 limits given by the hydraulic sensitivity analysis. In this case study, these values [*min*;*max*]  
382 are equal to [0.8;1.3] for the historical rating curve and [0.8;1.25] for the recent rating curve.  
383 Note that the choice of such a triangular distribution is somewhat arbitrary. Alternative  
384 assumptions may be used (e.g. O'Connel, 2005; O'Connel, et al., 2002). However, this choice  
385 is a delicate issue, since a hydraulic sensitivity analysis does not provide the full distribution  
386 of the rating curve error. This would require a more in-depth probabilistic assessment of the  
387 propagation of errors in the hydraulic model. This is considered to lie beyond the scope of this  
388 paper and is left for future work.

389

390 Lastly, Markov chain Monte Carlo (MCMC) algorithms are applied to the posterior  
391 distribution (12), making it possible to estimate the parameters and derived quantities,  
392 including flood quantiles. We used the two-stage MCMC strategy proposed by Renard *et al.*  
393 (2006b) . We refer to this paper for a detailed description of the algorithms used. Shortly, the  
394 first stage of the algorithm is an adaptive Gibbs sampler (Geman and Geman, 1984), which is  
395 used to perform a preliminary exploration of the posterior distribution properties (notably in  
396 terms of posterior covariance). In a second step, a standard Metropolis sampler (Metropolis  
397 and Ulam, 1949; Metropolis et al., 1953) is used, with a Gaussian jump distribution whose  
398 covariance matrix is specified using the preliminary exploration performed at stage one. The  
399 Metropolis sampler is ran during 100,000 iterations, with the first half of the iterations being  
400 considered as a burn-in period and being therefore discarded. Convergence was assessed by  
401 evolving four parallel chains and verifying that the Gelman-Rubin criteria (Gelman et al.,  
402 1995) were close to one for all inferred quantities.

403

### 404 **3. Results**

405

406 The modelled series (Figure 2) stems from two information sources: i) data from the flood  
407 warning gauge at Anduze (1892-2005), and ii) data from the historical survey, covering the  
408 1741-1891 period. The systematic period is exceptionally long at this site, lasting over 100  
409 years. Over the historical period, the perception threshold was taken to be 2961 m<sup>3</sup>/s,  
410 corresponding to the station's alert level. It should be remembered that discharge values are  
411 reconstructed on the basis of one recent (post-1985) and one historical (pre-1985) rating  
412 curve.

413

414 In a first step, the posterior distribution of GEV parameters obtained with the whole dataset  
415 (1741-2005) is evaluated. Figure 7 compares the posterior pdfs obtained when  
416 systematic/independent errors are accounted for (thick black lines) or ignored (thin grey  
417 lines). It shows that the location and scale parameters estimates are highly sensitive to the  
418 treatment of errors affecting data. Conversely, the shape parameter remains similar: this can  
419 be explained by the fact that the shape parameters of observed and true runoffs are identical  
420 (see appendix 1) with the error model (7) assumed in this study. The posterior pdfs of the  
421 multiplicative error terms  $\gamma_1$  and  $\gamma_2$  contain the value 1: the probabilistic model identifies no  
422 systematic rating curve error.

423 In a second step, the impact of additional historical information is evaluated by comparing  
424 quantiles obtained using the 1892-2005 data with quantiles obtained using the whole 1741-  
425 2005 dataset (Figure 8). Note that the treatment of systematic/independent errors is identical  
426 in both cases, with all errors being accounted for. Using historical data (pre-1892) appreciably  
427 changes the estimated quantiles, owing to the presence of many events in the vicinity of 4000  
428  $\text{m}^3/\text{s}$ . The fit with empirical frequencies is not very satisfactory, but given the shape suggested  
429 by these empirical frequencies, it seems likely that no curve would fit these points  
430 convincingly.

431

#### 432 **4. Sensitivity analysis**

433

434 Section 3 illustrated the impact of errors affecting discharge estimates when historical  
435 information is included in the inference. In this analysis, several quantities are fixed prior to  
436 the inference: (i) the width of the triangular prior (Figure 6) for systematic rating curve errors;  
437 (ii) the width of the discharge uncertainty intervals due to independent errors affecting water  
438 levels (intervals in figure 2); (iii) the value of the perception threshold. A sensitivity analysis

439 is carried out in this section to evaluate whether modifications of these predefined quantities  
440 significantly impact the estimated quantiles.

441

442 Sensitivity to the triangular prior for rating curve errors is studied by increasing/decreasing  
443 the width of the triangle base. More precisely, the original triangle with base  $[a;b]$  is replaced  
444 by a triangle with base  $[a';b']$  defined by:

445

$$\begin{aligned} a' &= a - z(1 - a) \\ b' &= b + z(b - 1) \end{aligned} \tag{14}$$

446

447  $z$  corresponds to an inflation factor. When  $z = 0$ , the interval  $[a;b]$  is unchanged; when  $z = 1$ ,  
448 the width of the interval is doubled; when  $z = -1$ , the interval collapses to the single point 1.  
449 The latter case yields a Dirac prior distribution, which corresponds to ignoring the rating  
450 curve systematic error.

451 Sensitivity to the intervals describing independent discharge errors ( $\varepsilon_i$ , equation (6)) makes  
452 use of a similar inflation factor, except that the value 1 in equation (14) is replaced by the  
453 centre of the interval  $[a;b]$ :

454

$$\begin{aligned} a' &= a - z((a + b)/2 - a) \\ b' &= b + z(b - (a + b)/2) \end{aligned} \tag{15}$$

455

456 Lastly, the sensitivity to the choice of the perception threshold  $u$  is studied by  
457 increasing/decreasing the value of  $u$ . When  $u$  is decreased, the historical information is  
458 preserved but its exhaustiveness occurs for a lower discharge. In some sense, decreasing the  
459 perception threshold therefore tests the robustness of the inference when the exhaustiveness

460 assessment is unduly optimistic. Conversely, when  $u$  is increased, all historical floods  
461 becoming smaller than  $u$  are discarded from the analysis.

462

463 Results from the sensitivity analysis are shown in figure 9 and yield interesting observations:

464 (i) The prior for rating curve systematic errors exerts a significant influence on the  
465 estimated quantiles. In particular, the uncertainty strongly increases with the prior  
466 width. This demonstrates the influence of the chosen prior distributions on the  
467 estimates, and calls for further research to derive meaningful priors from the  
468 hydraulic analysis.

469 (ii) Independent discharge errors stemming from imprecise knowledge of the water  
470 levels appear to impact the results to a lesser extent. In particular, ignoring these  
471 errors ( $z = -1$ ) leaves the original estimated quantiles ( $z = 0$ ) almost unchanged.

472 (iii) The choice of the perception threshold also exerts a significant influence on the  
473 inference, with the estimated quantiles being impacted by both increases and  
474 decreases of the threshold. As expected, the inference using historical information  
475 becomes similar to the inference solely using the data from the recent period when  
476 the threshold reaches high levels ( $u = 5,000$  or  $10,000 \text{ m}^3 \cdot \text{s}^{-1}$ ).

477

478 Although interesting, these observations should not be extrapolated beyond this particular  
479 case study. In particular, the relative influence of systematic and independent errors might be  
480 case-specific. This will be established in future work.

481

#### 482 **IV DISCUSSION**

483

484 The approach detailed for the Anduze catchment was also applied to the other four  
485 catchments of the Gard river listed in section 2. For all of these catchments, the following  
486 conclusions may be drawn. First, the use of historical data shows that Frechet-type  
487 distributions seem to represent flood discharge distributions better than the Gumbel  
488 distribution. For these catchments, the posterior distributions of the shape coefficient indicate  
489 that the coefficients are significantly different from zero, ranging from -0.25 at Alès to -0.5 at  
490 Anduze. The high values of the shape coefficient for the two main tributaries of the Gardon  
491 d'Anduze (Mialet and St-Jean) are consistent with the estimates at Anduze. We reach here the  
492 same conclusions as those obtained by Naulet *et al.* (2005) for the Ardèche river and  
493 Payrastre *et al.* (2005) for four catchments of the Aude river system. Thus, even when the  
494 systematic period is exceptionally long – over 100 years – the distributions of discharge  
495 values are clearly modified when historical floods are taken into account. Table 1 presents the  
496 estimates of the 10-year and 100-year quantiles for the four catchments with their respective  
497 confidence intervals. It can be seen that the ratio of the 100-year quantiles for the historical  
498 period to those for the systematic period ranges from 1.1 for the Gardon de Mialet to 1.85 for  
499 the Gardon d'Anduze at Anduze. This indicates once again the importance of taking historical  
500 flood data into consideration in the predetermination of flood volumes, even when long  
501 systematic time series are available.

502

503 Examination of the confidence intervals of the quantiles shows that, in contrast to what one  
504 might expect, these intervals can become wider when historical floods are taken into account  
505 compared to the systematic period alone. This result may be due to the high level of  
506 uncertainty affecting the highest historical floods and to the model used for systematic errors.

507

508 The specific 100-year flood discharge values obtained when the historical period is used  
509 range from 5 to 10 m<sup>3</sup>/s/km<sup>2</sup>, a standard order of magnitude for Mediterranean catchments.  
510 More specifically, we tried to compare our estimates of 100-year flood discharge (Q100) with  
511 other approaches (Table 2). The empirical relationships established for the Gard region by  
512 Bressand and Golosof (1996) give:

513

$$Q_{\text{rare}} = 30 A^{0.75} \quad \text{and} \quad Q_{\text{exc.}} = 50 A^{0.75} \quad (13)$$

514

515 where  $Q_{\text{rare}}$  and  $Q_{\text{exc.}}$  give orders of magnitude for 100-year and 1000-year flood discharge  
516 respectively, for a catchment with a surface area  $A$ .

517

518 Our estimates of Q100 using the historical data lie in an interval of -30% to +50% with  
519 respect to  $Q_{\text{rare}}$ . The historical 100-year flood discharge is higher than these estimates for the  
520 Anduze and Saint-Jean du Gard catchments. In addition, except in the case of the Gardon  
521 d'Anduze, these specific 100-year discharge values are below the highest regional curves of  
522 specific discharge values  $Q_{\text{max}}$  from major floods in Europe, constructed by Stanescu (2004)  
523 from a database of more than 700 flood events.

524 The specific discharge estimate of Q100 issued from a regional stochastic rainfall generator  
525 mixed with a rainfall-runoff model (Arnaud *et al.*, 2007), called Shyreg model, presents less  
526 variations among the four catchments. It seems more logical as the four basins have similar  
527 climatic and morphometric characteristics. Q100 estimates at Ales and Mialet are similar, as  
528 large differences between historical and Shyreg approaches are observed at St Jean (9,6  
529 versus 6,4) and especially at Anduze (9,5 versus 3,8). Large uncertainties on discharge  
530 estimates could explain such differences. Additional studies, based on both historical and



531 regional approaches, are needed to better understand the advantages and limits of each kind of  
532 information.

533

## 534 **V CONCLUSIONS**

535

536 A three-step procedure has been used to estimate discharge from major floods on the various  
537 Gardon catchments.

538

539 First, a historical survey identified and collected data on historical floods. The recent period is  
540 particularly rich in information on the studied catchments: the archives of daily discharge  
541 readings preserved by the flood forecasting department (FFD) allowed us to reconstruct the  
542 time series back to 1892, when the FFD was created. Information in the archives of the Gard  
543 region allowed us to supplement the Anduze time series with 29 unindexed flood events that  
544 occurred between 1741 and 1891. In view of this research, we can guarantee that the sample  
545 is complete for all floods since 1741 that exceeded the 1892 alert level.

546

547 These data were then used to reconstruct flood discharge series and their uncertainty, based on  
548 a hydraulic model. Several models were constructed for each site in order to take account, to  
549 the extent possible, of geomorphological changes in the riverbeds and changes in flood  
550 gauges during the period analysed. Recent and historical rating curves were constructed. For a  
551 given water level reading, they output a central discharge value with an uncertainty interval  
552 that takes account of the roughness of the channel in the reach considered. When this is  
553 cumulated with the uncertainty affecting water level readings, the overall uncertainty for the  
554 largest floods can be very high, with the relative error of the reconstructed discharge values  
555 reaching 100% in some cases.

556

557 Lastly, a Bayesian frequency analysis is performed in order to analyze the sample of recent  
558 and historical maxima, accounting for additive and multiplicative error affecting discharge  
559 values, respectively due to random error in water level readings and systematic rating curve  
560 error.

561

562 The use of historical flood data yielded mixed results. It lengthens the study period, but the  
563 reconstructed discharge values are in some cases subject to very high uncertainty, which is  
564 due among other things to the rating curves and affects recent discharge values as well. This  
565 demonstrates the need to improve discharge measurement, notably by increasing the number  
566 of flood gauges, so as to reduce the sources of uncertainty, at least for recent discharge values.  
567 When this uncertainty affecting discharge is taken into account in the probabilistic model, the  
568 confidence intervals for quantiles are in some cases higher when historical flood data are used  
569 than when the analysis is based solely on the recent discharge series. This demonstrates the  
570 need for careful evaluation of the various sources of uncertainty in order to assess the impact  
571 of using historical flood data and for their integration in the probabilistic model. In addition,  
572 the historical quantiles have been found of the same order of magnitude as those obtained  
573 through regional empirical methods, for two of the four studied catchments.

574

575

575 **Appendix 1**

576 The aim is to derive the distribution of  $\tilde{X}_t^{(k)} = X_t / \gamma_k - \varepsilon_t$ , conditionally on errors  $\gamma_k$  and  $\varepsilon_t$ .

577 For this purpose, let us write the cdf of  $\tilde{X}_t^{(k)}$  at a given value  $x$ :

$$\begin{aligned} \Pr(\tilde{X}_t^{(k)} \leq x) &= \Pr(X_t / \gamma_k - \varepsilon_t \leq x) \\ &= \Pr(X_t \leq \gamma_k(x + \varepsilon_t)) \end{aligned} \quad (16)$$

578 Since  $X_t \sim GEV(\mu, \lambda, \xi)$ , equation (1) yields:

$$\begin{aligned} \Pr(\tilde{X}_t^{(k)} \leq x) &= \Pr(X_t \leq \gamma_k(x + \varepsilon_t)) \\ &= \exp\left\{-\left[1 - \xi(\gamma_k(x + \varepsilon_t) - \mu) / \lambda\right]^{1/\xi}\right\} \\ &= \exp\left\{-\left[1 - \gamma_k \xi(x + \varepsilon_t - \mu / \gamma_k) / \lambda\right]^{1/\xi}\right\} \\ &= \exp\left\{-\left[1 - \xi(x - (\mu / \gamma_k - \varepsilon_t)) / (\lambda / \gamma_k)\right]^{1/\xi}\right\} \end{aligned} \quad (17)$$

579 The latter expression is equal to the cdf of a  $GEV(\mu / \gamma_k - \varepsilon_t, \lambda / \gamma_k, \xi)$  evaluated at  $x$ .

580

581 **Appendix 2**

582 The aim is to perform the following integration:

$$p(\tilde{X}_t^{(k)} | \mu, \lambda, \xi, \gamma_k) = \int p(\tilde{X}_t^{(k)} | \mu, \lambda, \xi, \gamma_k, \varepsilon_t) p(\varepsilon_t) d\varepsilon_t \quad (18)$$

583 Assuming  $p(\varepsilon_t)$  is a uniform distribution on  $[a_t, b_t]$  yields:

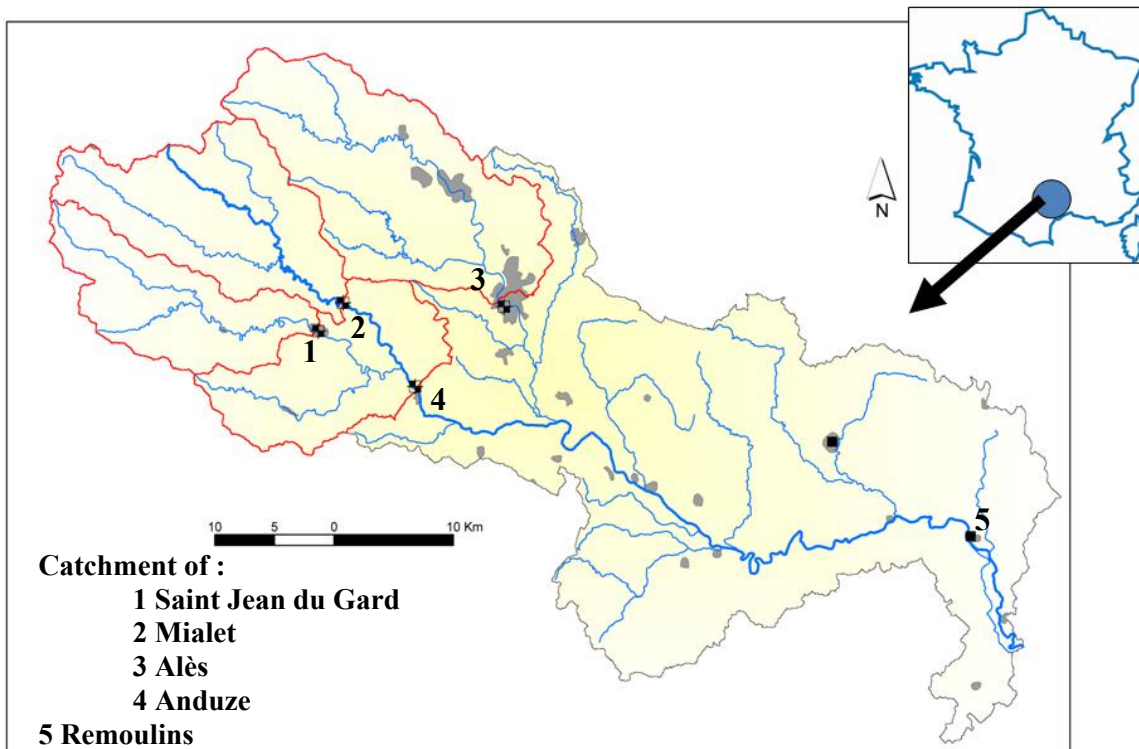
$$\begin{aligned} p(\tilde{X}_t^{(k)} | \mu, \lambda, \xi, \gamma_k) & \\ &= \int_{a_t}^{b_t} f(\tilde{x}_t^{(k)} | \mu / \gamma_k - \varepsilon_t, \lambda / \gamma_k, \xi) \frac{1}{b_t - a_t} d\varepsilon_t \\ &= \frac{1}{b_t - a_t} \int_{a_t}^{b_t} (\gamma_k / \lambda) \left[1 - \xi \gamma_k (\tilde{x}_t^{(k)} - \mu / \gamma_k + \varepsilon_t) / \lambda\right]^{\frac{1}{\xi} - 1} \exp\left\{-\left[1 - \xi \gamma_k (\tilde{x}_t^{(k)} - \mu / \gamma_k + \varepsilon_t) / \lambda\right]^{1/\xi}\right\} d\varepsilon_t \end{aligned} \quad (19)$$

584 Using the substitution  $u = \tilde{x}_t^{(k)} + \varepsilon_t$ :

$$\begin{aligned}
 & p(\tilde{X}_t^{(k)} | \mu, \lambda, \xi, \gamma_k) \tag{20} \\
 &= \frac{1}{b_t - a_t} \int_{\tilde{x}_t^{(k)} + a_t}^{\tilde{x}_t^{(k)} + b_t} (\gamma_k / \lambda) [1 - \xi \gamma_k (u - \mu / \gamma_k) / \lambda]^{\frac{1}{\xi} - 1} \exp\left\{-[1 - \xi \gamma_k (u - \mu / \gamma_k) / \lambda]^{1/\xi}\right\} du \\
 &= \frac{1}{b_t - a_t} \int_{\tilde{x}_t^{(k)} + a_t}^{\tilde{x}_t^{(k)} + b_t} f(u | \mu / \gamma_k, \lambda / \gamma_k, \xi) du \\
 &= \frac{1}{b_t - a_t} \left[ F(\tilde{x}_t^{(k)} + b_t | \mu / \gamma_k, \lambda / \gamma_k, \xi) - F(\tilde{x}_t^{(k)} + a_t | \mu / \gamma_k, \lambda / \gamma_k, \xi) \right]
 \end{aligned}$$

585

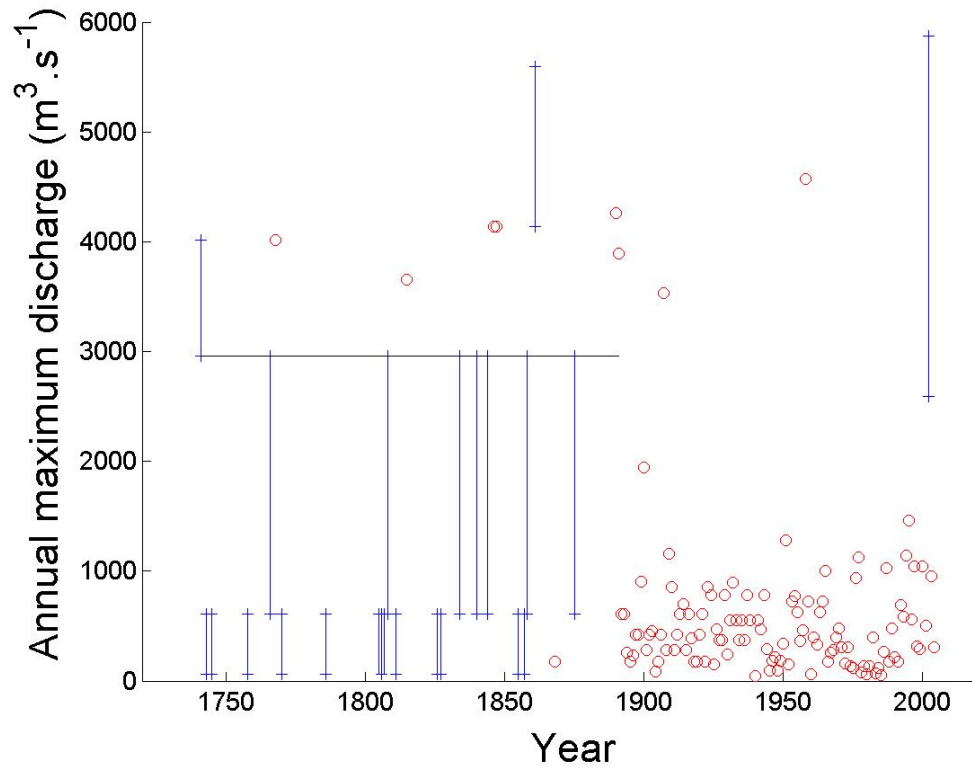
585



586

587 **Figure 1: Overview of the four studied catchments**

588

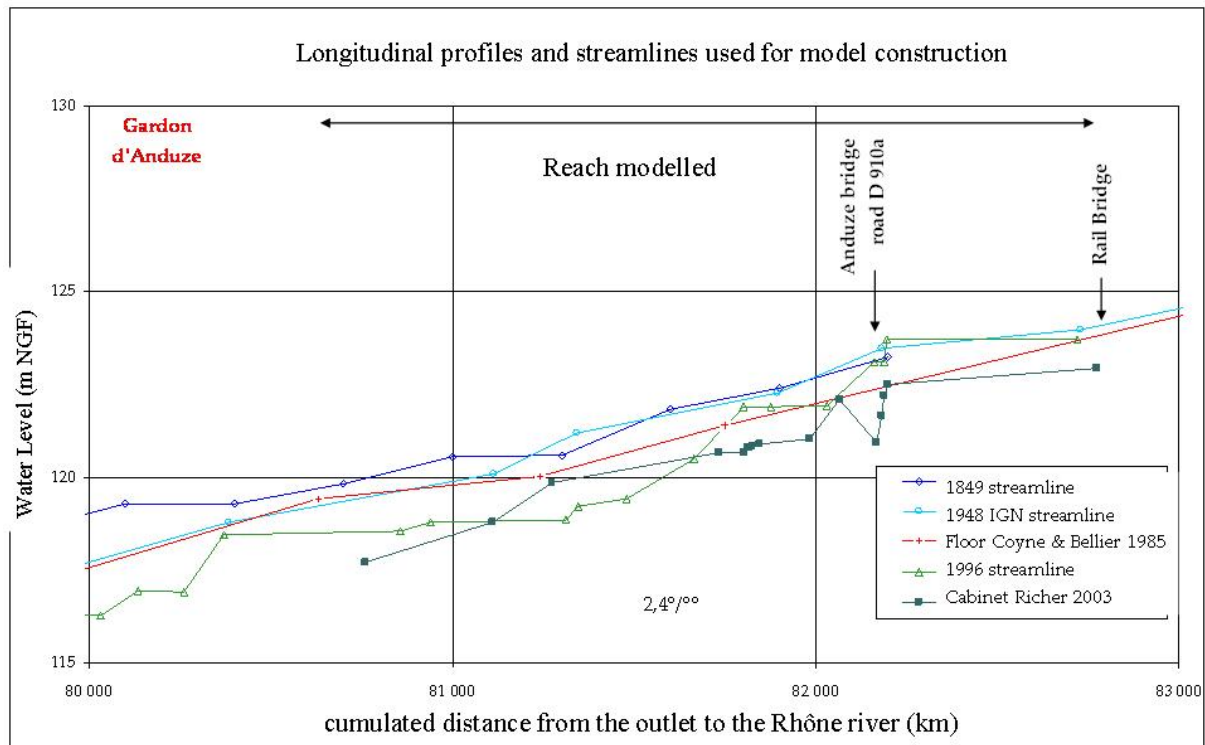


588

589 **Figure 2: Floods on the Gardon d'Anduze river at Anduze (1741-2005). Circles correspond to events**  
590 **whose water level is known with high precision. Intervals represent the uncertainty due to imperfect**  
591 **knowledge of the water level reached during the event. The horizontal line is the perception threshold.**

592

592

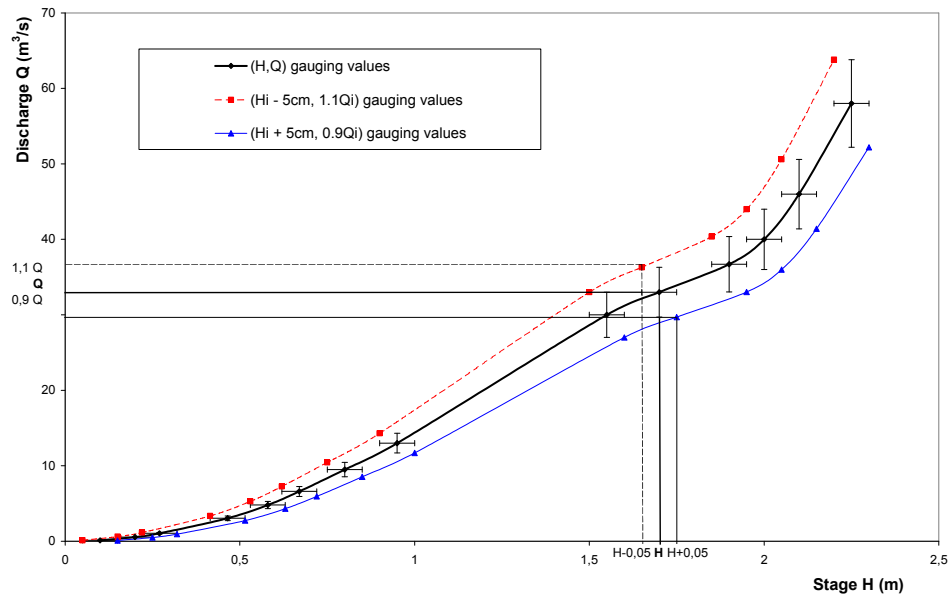


593

594 **Figure 3: Longitudinal profile of the Gardon d'Anduze river at Anduze**

595

596



597 **Figure 4: Envelope curves of the stage-discharge relationship**

598

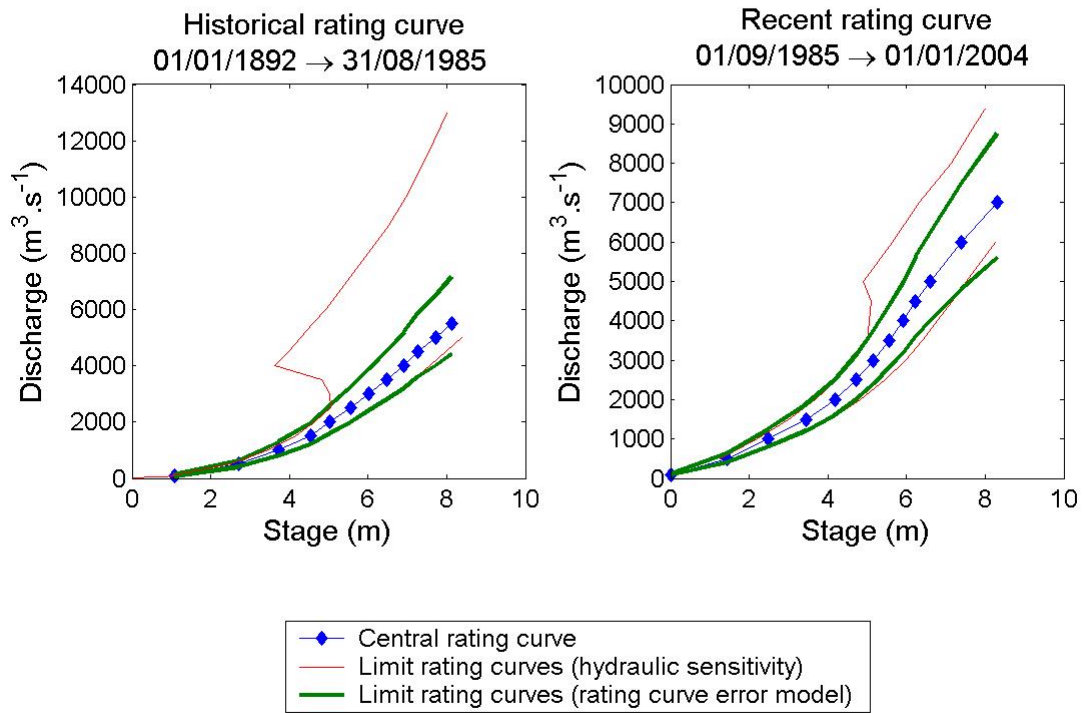
599



599

600

601



602

603

604 **Figure 5: Historical and recent rating curves**

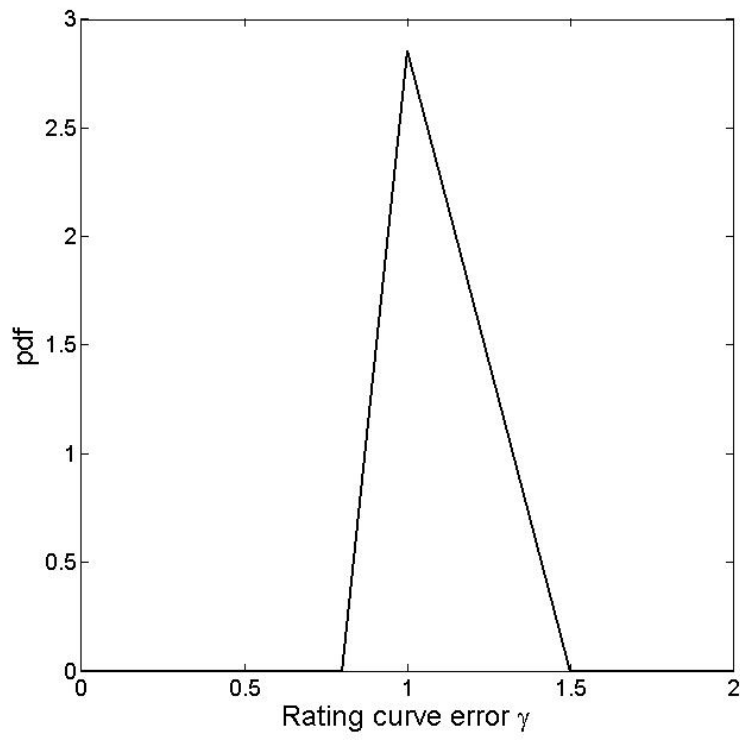
605

605

606

607

608



609

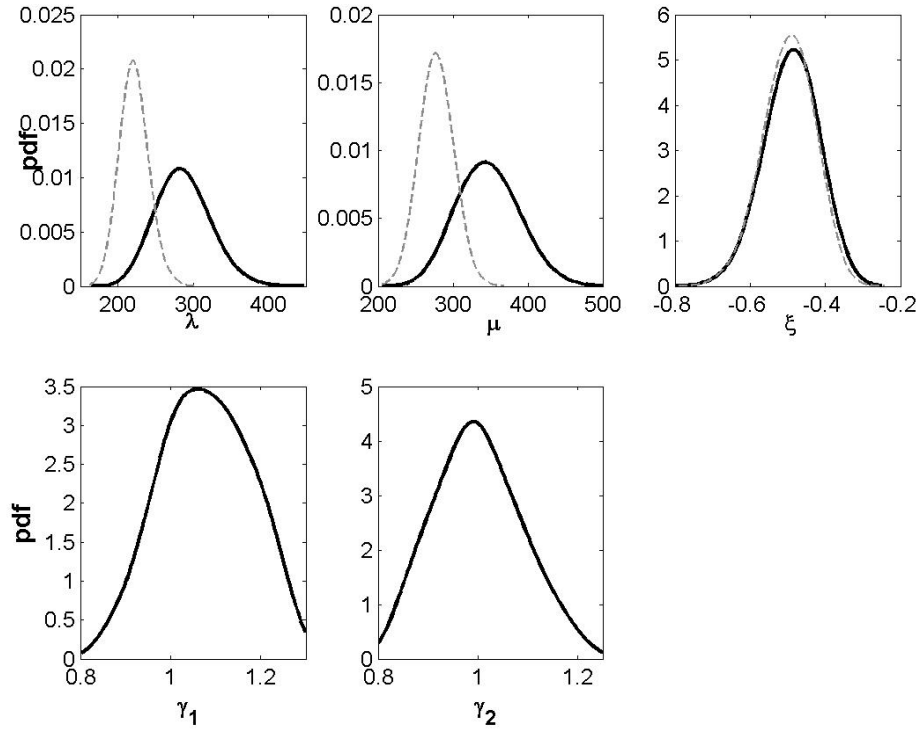
610

611 **Figure 6: Illustration of a triangular prior pdf for the rating curve error parameter  $\gamma$**

612

612

613



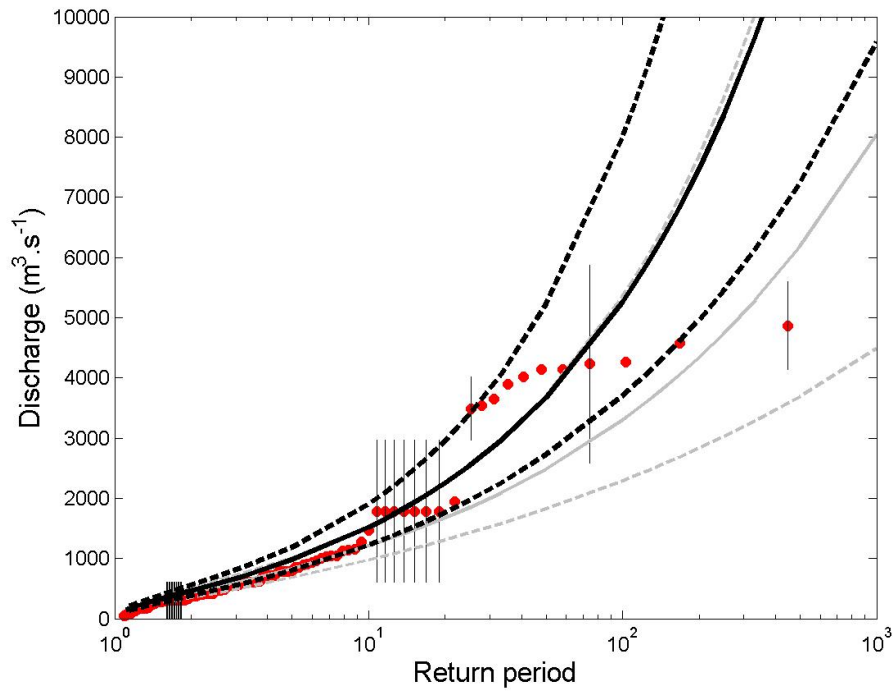
614

615 **Figure 7: Posterior pdfs of GEV parameters  $\lambda$ ,  $\mu$ ,  $\xi$ , and of rating curve error parameters  $\gamma_1$  and  $\gamma_2$ ,**

616 **obtained with the whole dataset 1741-2005. Thick black lines = systematic and independent errors**

617 **accounted for; thin grey lines: systematic and independent errors ignored.**

618



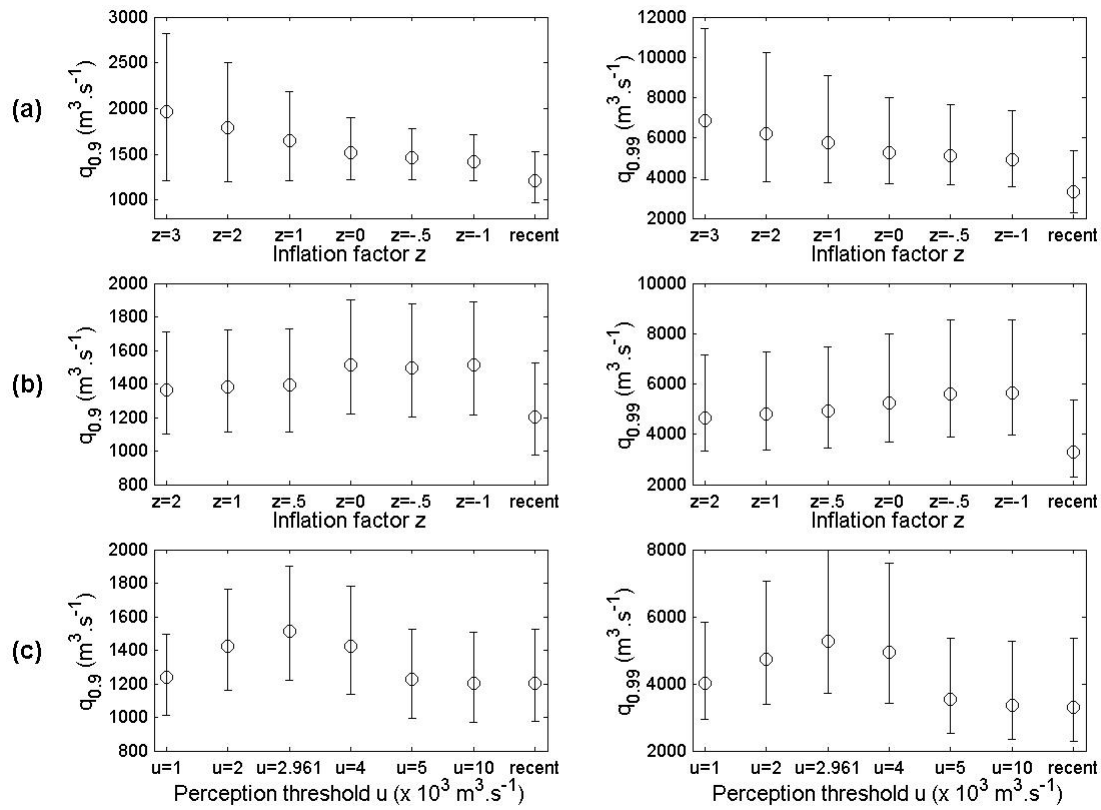
618

619 **Figure 8: GEV distribution of annual maxima at Anduze, with 90% posterior intervals**

620 Note: Thick lines = whole period (1741-2005); thin lines = the systematic period (1892-2005); circles =  
621 empirical frequencies.

622

622



623

624 **Figure 9: Sensitivity of 0.9- and 0.99-quantiles posterior estimates. Circles represent posterior medians,**  
 625 **bars represent 90% posterior intervals. (a) Sensitivity to the prior for systematic rating curve errors; (b)**  
 626 **sensitivity to the width of intervals describing independent errors; (c) sensitivity to the perception**  
 627 **threshold. ‘recent’ denotes results with data from the period 1892-2005 (with rating curve errors**  
 628 **accounted for).**

629

630

630

631

Catchment (area)	Systematic period		Historical period	
	Q10 +/- IC 90% (m <sup>3</sup> /s)	Q100 +/- IC 90% (m <sup>3</sup> /s)	Q10 +/- IC90% (m <sup>3</sup> /s)	Q100 +/- IC90% (m <sup>3</sup> /s)
Anduze (540 km <sup>2</sup> )	1070 +240/-170	2780 +1680/-800	1460 +360/-290	5130 +2650/-1540
Alès (320 km <sup>2</sup> )	690 +370/-80	1330 +550/-530	770 +130/-120	1650 +480/-340
Mialet (219 km <sup>2</sup> )	250 +90/-60	1170 +1110/-460	270 +80/-60	1250 +770/-420
Saint-Jean (154 km <sup>2</sup> )	300 +80/-60	920 +680/-300	360 +100/-70	1480 +900/-480

632

633 **Table 1: 10-year and 100-year quantiles in m<sup>3</sup>/s estimated on the basis of the systematic and historical**  
 634 **periods, and their 90% confidence intervals**

635 ]

636

637

638

639

640

641

Catchments (area)	Q100 with historical data	Q <sub>rare</sub>   Q <sub>exc.</sub> (Bressand and Golossov, 1996)	Q <sub>max</sub> (Stanescu, 2004)	Shyreg (Arnaud and Lavabre, 2007)
Anduze (540 km <sup>2</sup> )	9.5	6.2   10.4	7.8	3.8
Alès (320 km <sup>2</sup> )	5.2	7.1   11.8	10	5.1
Mialet (219 km <sup>2</sup> )	5.7	7.8   13.0	12.8	5.4
Saint- Jean (154 km <sup>2</sup> )	9.6	8.5   14.2	13.9	6.4

642

643 **Table 2: Comparison of specific discharge estimates (m<sup>3</sup>/s.km<sup>2</sup>) for 100-year quantiles or major floods on**  
 644 **the Gardon rivers**

645

646

647

648

648 **Bibliographical references**

649

650 Arnaud P., Lavabre J., Sol B., Desouches C., 2007. Régionalisation d'un générateur de pluies  
651 horaires sur la France métropolitaine pour la connaissance de l'aléa pluviographique.  
652 *Hydrological Sciences Journal*, 53 (1), 34-47.

653

654 Ayrat P.A., 2005. Contribution à la spatialisation du modèle opérationnel de prévision des  
655 crues éclair ALTHAIR, approches spatiale et expérimentale ; application au bassin versant  
656 du Gardon d'Anduze. MSc Thesis, University d'Aix Marseille, 311 p.

657

658 Barnes H.H., 1967. Roughness Characteristics of Natural Channels. U.S. Geological Survey,  
659 Water Supply Paper 1849.  
660 <http://wwwrcamnl.wr.usgs.gov/sws/fieldmethods/Indirects/nvalues/index.htm>

661

662 Brazdil R., Kundzewicz Z.W., Benito G., 2006. Historical hydrology for studying flood risk  
663 in Europe. *Hydrological Sciences Journal*, 51 (5), 739-764.

664

665 Bressand F., Golossov G., 1996. Méthode de calcul des débits rares et exceptionnels d'eaux  
666 pluviales sur les petits bassins versants naturels situés dans l'arc méditerranéen. DDE  
667 (Infrastructure Department) for the Gard region (France), Water and Environment unit, 42 pp.

668

669 Chow, V.T., 1960. Open Channel hydraulics, Mc Graw Hill Book Company, New-York,  
670 380p.

671



- 672 Cœur D., Lang M., Paquier A., 2002. L'historien, l'hydraulicien et l'hydrologue et la  
673 connaissance des inondations. *La Houille Blanche*, 4/5, 61-66.  
674
- 675 Coles, S. G., and E. A. Powell, 1996. Bayesian methods in extreme value modelling: A  
676 review and new developments, *Int. Stat. Rev.*, 64, 119-136.  
677
- 678 DDE (*Direction Départementale de l'Équipement* – Infrastructure Department) of the Gard  
679 region (France), 2003. Validation des relevés hydrométriques de la crue du 08 et 09  
680 septembre 2002. SOGREAH internal report, no. 102793, November 2003, 98 pp.  
681
- 682 Delrieu G., Kirstetter P-E., Nicol J., Neppel L., 2004. L'événement pluvieux des 08 et 09  
683 septembre 2002 dans le Gard : estimation des précipitations par radars et pluviomètres. *La*  
684 *Houille Blanche*, 6, 93-98.  
685
- 686 Embrecht C., Kluppelberg C., Mikosch T., 1997. *Modelling Extremal Events for Insurance*  
687 *and Finance*. Springer-Verlag, Berlin.  
688
- 689 Gaume E., Livet M., Desbordes M., Villeneuve J.P., 2004. Hydrological analysis of the river  
690 Aude, France, flash flood on 12 and 13 November 1999. *Journal of Hydrology*, 286, 135-154.  
691
- 692 Gelman, A., et al., 1995. *Bayesian data analysis*, 526 pp., Chapman & Hall.  
693
- 694 Gob F., Jacob N., Bravard J.P., Petit F., 2008. The value of lichenometry and historical  
695 archives in assessing the incision of submediterranean rivers from the Little Ice Age in the  
696 Ardèche and upper Loire (France). *Geomorphology*, 94, 170-183.

697

698 Hirsh R.M., Stedinger J.R., 1987. Plotting positions for historical floods and their precision.  
699 *Water Resources Research*, 22(4), 715-727.

700

701 Huet P., Martin X., Prime J.L., Foin P., Laurain C., Cannard P., 2003. Retour d'expérience  
702 des crues de septembre 2002 dans les départements du Gard, de l'Hérault, du Vaucluse, des  
703 Bouches du Rhône, de l'Ardèche et de la Drôme. Report of the General Inspectorate for the  
704 Environment, Ministry of Ecology, Energy, Sustainable Development and Regional Planning  
705 (MEEDDAT), 133 pp.

706 <http://www.ecologie.gouv.fr/-Rapports-de-l-Inspection-generale-.html>.

707

708 ISL Bureau d'Ingenieurs Conseils, 2005. Référentiel hydrologique sur le bassin versant des  
709 Gardons. DDE (Infrastructure Department) of the Gard region, internal report.

710

711 Jacquet J., 1959. Les crues d'automne 1958 sur le Vidourle. *Mémoire et travaux de la société*  
712 *hydrotechnique de France*, (1)11: 66-82.

713

714 Kuczera, G., 1992. Uncorrelated measurement error in flood frequency inference, *Water*  
715 *Resources Research*, 28, 183-188.

716

717 Kuczera, G., 1996. Correlated rating curve error in flood frequency inference, *Water*  
718 *Resources Research*, 32, 2119-2127.

719

720 Lang M., Perret C., Renouf E., Sauquet E., Paquier A., 2006. Incertitudes sur les débits de  
721 crue. *La Houille Blanche*, 6, 33-41

722

723 Llasat C., Barriendos M., Barrera A., Rigo T., 2005. Floods in Catalonia (NE Spain) since the  
724 14th century. Climatological and meteorological aspects from historical documentary sources  
725 and old instrumental records. *Journal of Hydrology*, 313, 32-47.

726

727 Martins, E. S., and J. R. Stedinger, 2000. Generalized maximum-likelihood generalized  
728 extreme-value quantile estimators for hydrologic data, *Water Resources Research*, 36, 737-  
729 744.

730

731 Naulet R., 2002. Utilisation de l'information des crues historiques pour une meilleure  
732 prédétermination du risque d'inondation. Application au bassin de l'Ardèche à Vallon Pont  
733 d'Arc et à St Martin d'Ardèche. PhD diss., Université Joseph Fourier Grenoble, Université du  
734 Québec INRS, Cemagref Lyon, 322 pp.

735

736 Naulet R., Lang M., Ouarda Taha B.M.J., Coeur D., 2005. Flood frequency analysis on the  
737 Ardèche river using French documentary sources from the last two centuries. *Journal of*  
738 *Hydrology*, 313, 58-78.

739

740 Neppel L., Bouvier C., Vinet F., Desbordes M., 2003. Sur l'origine de l'augmentation des  
741 inondations en région méditerranéenne. *Revue des Sciences de l'Eau*, 16 (4), 475-494.

742

743 Neppel L. *et al.*, 2007. InondHis-LR : analyse des précipitations et crues anciennes en région  
744 Languedoc-Roussillon. RDT programme, Ministry of Ecology, Energy, Sustainable  
745 Development and Regional Planning (MEEDDAT), contract CV04000067, 209 pp.

746

- 747 Marchandise A., 2007. Modélisation hydrologique distribuée sur le Gardon d'Anduze ; étude  
748 comparative de différents modèles pluie-débit, extrapolation de la normale à l'extrême et tests  
749 d'hypothèses sur les processus hydrologiques, MSc Thesis. University Montpellier II,  
750 Montpellier, France.
- 751
- 752 O'Connel, D. R. H., 2005. Nonparametric Bayesian flood frequency estimation, *J. Hydrol.*,  
753 *313*, 79-96.
- 754
- 755 O'Connel, D. R. H., Ostenaar D.A., Levish R., Klinger R.E., 2002. Bayesian flood frequency  
756 analysis with paleohydrologic bound data, *Water Resources Research*, *38*.
- 757
- 758 Paquier A., Khodashenas S.R., 2002. River bed deformation calculated from boundary shear  
759 stress. *Journal of Hydraulic Research*, *40* (5), 603-609.
- 760
- 761 Parent, E., and J. Bernier, 2003. Bayesian POT modeling for historical data, *J. Hydrol.*, *274*,  
762 95-108.
- 763
- 764 Payrastre O., Gaume E., Andrieu H., 2005. Use of historical data to assess the occurrence of  
765 floods in small watersheds in the French Mediterranean Area. *Advances in Geosciences*, *2*,  
766 313-320.
- 767
- 768 Payrastre O., Gaume E., Andrieu H., 2006. Apport du recueil de données historiques pour  
769 l'étude des crues extrêmes de petits cours d'eau ; Etude du cas de quatre bassins versants  
770 affluents de l'Aude. *La Houille Blanche*, *6*, 79-86.
- 771

- 772 Reis, D. S., and J. R. Stedinger, 2005. Bayesian MCMC flood frequency analysis with  
773 historical information, *J. Hydrol.*, 313, 97-116.  
774
- 775 Reitan, T., and A. Petersen-Overleir, 2009. Bayesian methods for estimating multi-segment  
776 discharge rating curves, *Stochastic Environmental Research and Risk Assessment*. 23(5), 627-  
777 642  
778
- 779 Renard B., 2006. Détection et prise en compte d'éventuels impacts du changement climatique  
780 sur les extrêmes hydrologiques en France. PhD diss., INP Grenoble, Cemagref Lyon, 361 pp.  
781
- 782 Renard, B., M. Lang, and P. Bois, 2006a. Statistical analysis of extreme events in a non-  
783 stationary context via a Bayesian framework., *Stoch. Environ. Res. Risk Assess.*, 21, 97-112.  
784
- 785 Renard B., Garreta V., Lang M., 2006b. An application of Bayesian analysis and MCMC  
786 methods to the estimation of a regional trend in annual maxima. *Water Resources Research*,  
787 42.  
788
- 789 Renouf E., Lang M., Sauquet E., Paquier A., 2005. Contrôle de la qualité des courbes de  
790 tarage de la banque HYDRO pour les débits de crue. Cemagref report for the Ministry of  
791 Ecology and Sustainable Development (MEDD), 53 pp. + annexes (112 pp.).  
792
- 793 Ribatet, M., E. Sauquet, J. M. Gresillon, and T. B. M. J. Ouarda, 2006. A regional Bayesian  
794 POT model for flood frequency analysis, *Stoch. Environ. Res. Risk Assess.*, 21, 327-339.  
795

796 Sheffer N.A., Rico M., Enzel Y., Benito G., Grodrek T., 2008. The paleoflood record of the  
797 Gardon River, France: A comparison with the extreme 2002 flood event. *Geomorphology* 98,  
798 71-83, doi:10.1016/j.geomorph.2007.02.034.

799

800 Stanescu V.A., 2004. Le potentiel des grandes crues de l'Europe, leur régionalisation et  
801 comparaison. *La Houille Blanche*, 6, 21-25.

802

803 Thyer, M., B. Renard, D. Kavetski, G. Kuczera, S.W. Franks and S.W. Srikanthan, ?? 2009.  
804 Critical evaluation of parameter consistency and predictive uncertainty in hydrological  
805 modelling: a case study using bayesian total error analysis, *Water Resources Research*, 45.

806 W00B14

807